

Direct Signal Separation Via Extraction of Local Frequencies with Adaptive Time-Varying Parameters*

Lin Li¹, Charles K. Chui² and Qingtang Jiang³

Jan 18, 2020

Submitted to IEEE Trans SP on Jan 21, 2020, ms # T-SP-26004-2020

1. School of Electronic Engineering, Xidian University, Xi'an, China
2. College of Mathematics and Statistics, Shenzhen University, China
and Department of Mathematics, Hong Kong Baptist University, China
3. Department of Math & CS, University of Missouri-St. Louis, St. Louis, MO, USA

Abstract

In nature, real-world phenomena that can be formulated as signals (or in terms of time series) are often affected by a number of factors and appear as multi-component modes. The natural approach to understand and process such phenomena is to decompose, or even better, to separate the multi-component signals to their basic building blocks (called sub-signals or time-series components, or fundamental modes) for extracting the necessary features such as volatility, trends, outliers, and the underlying dynamics. However, since such signals are mainly non-stationary, there has been no effective rigorous methods available for decomposition of such multi-component signals, except the popular ad hoc computational scheme, called empirical mode decomposition (EMD). The essence of EMD is first to decompose the blind-source signal into a sum of components, called intrinsic mode functions (IMFs) with some residue function, called the trend; followed by extracting the instantaneous frequencies (IFs) of the IMFs. On the other hand, for stationary signals there is the classic work of De Prony (called Prony's method), and its improvements to the well-known MUSIC and ESPRIT algorithms, based on the mathematical model of exponential sums (in terms of constant frequencies), for first extracting the frequencies, from which the sub-signals are recovered. We may call this a time-frequency approach for signal separation. The difference between EMD for signal decomposition and the time-frequency approach for signal separation, is that signal decomposition is applied before frequencies are estimated, while frequencies are first extracted before the multi-component signal is separated. Hence, for the time-frequency approach, the wavelet synchro-squeezing transform (SST) and its variants may be considered as an advancement of Prony's method from separation of stationary signals to that of nonstationary signals. More recently, a direct method of the time-frequency approach, called signal separation operation (SSO), was introduced to solving the inverse problem of multi-component signal separation. While both SST and SSO are mathematically rigorous on IF estimation, SSO

*This work is partially supported by the Hong Kong Research Council, under Projects # 12300917 and # 12303218, and HKBU Grants # RC-ICRS/16-17/03 and # RC-FNRA-IG/18-19/SCI/01, and by the Simons Foundation, under grant # 353185.

avoids the second step of the two-step SST method in signal separation, which depends heavily on the accuracy of the estimated IFs. In the present paper, we solve the inverse problem by constructing an adaptive signal separation operator (ASSO) for more effective separation of the blind-source multi-component signal, via introducing a time-varying parameter that adapts to local IFs. A recovery scheme is also proposed to extract the signal components one by one, and the time-varying parameter is updated for each component. The proposed method is suitable for engineering implementation, being capable of separating complicated signals into their sub-signals and reconstructing the signal trend directly. Numerical experiments on synthetic and real-world signals are presented to demonstrate our improvement over the previous attempts.

1 Introduction

For radar, communication, and other applications, a non-stationary multi-component signal $x(t)$ is usually represented as a superposition of Fourier-like oscillatory amplitude-frequency modulated (AM-FM) components, called the AM-FM model [1, 2]. Motivated by the empirical mode decomposition (EMD) [3], we model a non-stationary multi-component signal (or in terms of a time series) by

$$x(t) = \sum_{k=1}^K x_k(t) + A_0(t) = F(t) + A_0(t), \quad (1)$$

$$F(t) = \sum_{k=1}^K x_k(t) = \sum_{k=1}^K A_k(t) \cos(2\pi\phi_k(t)), \quad (2)$$

where $A_0(t)$, called the trend of $x(t)$, is (at most) minimally oscillatory. The function $F(t)$ in (2) with $0 < \mu \leq A_k(t) \leq M$, $\phi'_k(t) \geq 0$ and $\phi'_k(t) > 0$ almost everywhere (a. e.), $\phi'_k(t) > \phi'_{k-1}(t)$, and $A_k(t)$, $\phi'_k(t)$ varying more slowly than $\cos(2\pi\phi_k(t))$ (see [4], Eq.(1.3)), is called the AF-FM model, where $A_k(t)$ are called the instantaneous amplitudes (IAs) and $\phi'_k(t)$ the instantaneous frequencies (IFs), which can be used to describe the underlying dynamics. $F(t)$ is also called the “adaptive harmonic model” (AHM) in current mathematics literature (see for example [4, 5, 6]).

The EMD is a popular method for decomposition of a non-stationary signal as a superposition of IMFs that satisfy two conditions: (a) the number of its local minima and local maxima must either be equal or differ at most by one; and (b) the value of the mean of its upper envelope and lower envelope is close to zero. Then the instantaneous frequency (IF) of each IMF is calculated, first by applying the Hilbert transform to compute its imaginary conjugate so as to extend the IMF from the time-domain to an analytic signal in the upper half of the complex plane, and secondly by re-formulating the analytic signal in its polar form, and finally by taking the real part to obtain the instantaneous amplitude and IF of each component. EMD is an efficient data-driven approach and no basis of functions is used. It has been widely used in many applications, see [7] and the references therein. There are many articles studying the property of EMD or proposing variants of EMD to improve the performance, see e.g. [8]-[16]. In particular, the separation ability of EMD is discussed in [10], which shows that EMD cannot decompose two components when their frequencies are close to each other. The ensemble EMD (EEMD) is proposed to suppress the noise interference

[11]. A weakness of EMD or EEMD is that it can easily lead to mode mixture or artifacts, namely undesirable or false components [12]. An EMD-like sifting process is recently proposed in [16], which extracts components in the linear time-frequency (TF) plane one by one.

It is important to point out our objective of signal separation is to solve an inverse problem which is quite different from EMD. EMD is an ad hoc computational scheme for decomposing a non-stationary signal into its “IMFs” and “trend”, without the concern of recovering the true IMF and trend of the source signal. For stationary signals there is the classic work of De Prony (called Prony’s method) [17], and its improvements to the well-known MUSIC [18] and ESPRIT [19] algorithms, based on the mathematical model of exponential sums (in terms of constant frequencies), for first extracting the frequencies, from which the sub-signals are recovered. We may call this a time-frequency approach for signal separation. The difference between EMD for signal decomposition and the time-frequency approach for signal separation, is that signal decomposition is applied before frequencies are estimated, while frequencies are first extracted before the multi-component signal is separated.

The linear TF analysis with a reversible transform is also a powerful tool for analyzing time-varying non-stationary signals [20, 21]. The synchrosqueezed wavelet transform (SST), introduced in [22] and recently developed in [5] provides mathematical theorems to guarantee the recovery of oscillatory modes, IFMs from the source signal $F(t)$. SST and all later developments, including [23]-[33] and the short-time Fourier transform (STFT)-based SSTs [34]-[38], re-assign the scale variable (for continuous wavelet transform-based SST) or the frequency variable (for STFT-based SST) to sharpen the time-frequency representation of a signal. In addition, very recently the authors of [39, 40] proposed the adaptive WSST and adaptive FSST with a time-varying adaptive Gaussian window. They obtain the well-separated conditions for multicomponent signals using the linear frequency modulation to approximate a non-stationary signal at any local time, along with a new definition of bandwidth of Gaussian window. The SST and its variants may be considered as an advancement of Prony’s method from separation of stationary signals to that of nonstationary signals.

To obtain IMFs, the SST method consists of two steps. IFs are estimated from the SST plane. After recovering of IFs, the IMFs of the source signal are computed by reversible transforms along each estimated IF curves on the SST plane.

On the other hand, [4] introduced a new method with signal separation operator (SSO) to solving the inverse problem of multi-component signal separation. We called this method SSO method. While both SST and SSO are mathematically rigorous on IF estimation, SSO avoids the second step of the two-step SST method in signal separation, which depends heavily on the accuracy of the estimated IFs. In the SSO approach, the IMFs are reconstructed simply by substituting the time-frequency ridge to SSO.

A window function is used in SSO. The window function in [4] has the same window length for all the components (sub-signals). In this paper we introduce and construct an adaptive signal separation operator (ASSO) which separates the original signal by the local frequencies directly. We adopt a time-varying window for adaptive separation of each sub-signal by the proposed ASSO.

The main innovations of this paper are: (a) we proposed a more accurate component recovery formula; (b) we proposed a recovery scheme to extract the signal components one by one, and the time-varying window is updated for each component; (c) the proposed separation algorithm is capable of separating much complicated multicomponent signals and reconstructing the signal trend directly, and (d) the proposed method is suitable for engineering implementation with truncated Gaussian window and fast Fourier transform (FFT).

The remainder of the paper is organized as follows. We review the basic theory of signal separation by time-frequency analysis briefly in Section 2. In Section 3, we formulate and state the results on the proposed ASSO. We obtain the relationship between the SSO and the STFT with a time-varying parameter. In Section 4, we analyze the component recovery error when the window function is the Gaussian window function, and we provide a component recovery formula which is more accurate than that by the original SSO. In Section 5, we present the numerical experiments on synthetic data and measured data. Our experimental results show that ASSO outperforms the EMD and SSTs in estimation of IFs and signal separation. Finally, we give a brief conclusion in Section 6.

2 Signal separation by time-frequency analysis

The modified STFT of a signal $x(t) \in L_2(\mathbb{R})$ with a window function $h(t) \in L_2(\mathbb{R})$ is defined by

$$V_x(t, \eta) := \int_{\mathbb{R}} x(\tau)h(\tau - t)e^{-j2\pi\eta(\tau - t)}d\tau, \quad (3)$$

where t and η are the time variable and the frequency variable respectively. For a real-valued window function $h(t)$ with $h(0) \neq 0$, one can show that a real-valued signal $x(t)$ can also be recovered back from its STFT $V_x(t, \eta)$ with integrals involving only η :

$$x(t) = \frac{2}{h(0)}\text{Re}\left(\int_{-\infty}^{\infty} V_x(t, \eta)d\eta\right). \quad (4)$$

Here we remark that if the window function $h(t)$ is in the Schwarz class, then STFT $V_x(t, \eta)$ of a slowly growing $x(t)$ with $h(t)$ is well defined. Furthermore, and the above formula still holds.

Note that to recover/separate the components $x_k(t)$ of a multicomponent signal as given in (1) from its STFT, if $V_{x_{k-1}}(t, \eta)$ and $V_{x_k}(t, \eta)$ of two components $x_{k-1}(t)$ and $x_k(t)$ are ‘‘mixed’’ (the contrary case of ‘‘separated’’, see (6) for example), then it cannot separate these two components, and hence it cannot recover/separate them accurately.

When $x_k(t)$ are sinusoidal signals $x_k(t) = A_k e^{j2\pi c_k t}$ for some constants $A_k, c_k > 0$, or they are well approximated by sinusoidal functions in a small neighborhood of a fixed $t \in \mathbb{R}$, namely at any local time of t ,

$$\begin{aligned} x_k(t + \tau) &= A_k(t + \tau)e^{j2\pi\phi_k(t + \tau)} \\ &\approx A_k(t)e^{j2\pi(\phi_k(t) + \phi'_k(t)\tau)} = x_k(t)e^{j2\pi\phi'_k(t)\tau}, \end{aligned} \quad (5)$$

for small τ , then the STFT $V_{x_k}(t, \eta)$ of $x_k(t)$ with a window function $h(t)$ is

$$V_{x_k}(t, \eta) \approx x_k(t)\widehat{h}(\eta - \phi'_k(t)),$$

where \widehat{h} denotes the Fourier transform of $h(t)$.

Since the support zone of $V_{x_k}(t, \eta)$ is determined by the support of \widehat{h} , we need to define the *essential support* of \widehat{h} if h is not band-limited. More precisely, for a given threshold $0 < \tau_0 < 1$ small enough, if $|\widehat{h}(\xi)| / \max_{\xi} |\widehat{h}(\xi)| \leq \tau_0$ for $|\xi| \geq \lambda_h$, then we say $\widehat{h}(\xi)$ is *essentially supported* in $[-\lambda_h, \lambda_h]$. Note that $\lambda_h = \lambda_{h, \tau_0}$ depends on τ_0 . For simplicity, here and below we drop the subscript τ_0 .

Hence if $\text{supp}(\widehat{h}) \subseteq [-\lambda_h, \lambda_h]$ for some $\lambda_h > 0$, then $V_{x_k}(t, \eta)$ lies in the time-frequency zone given by

$$Z_k := \{(t, \eta) : |\eta - \phi'_k(t)| < \lambda_h, t \in \mathbb{R}\}.$$

Therefore, if

$$\phi'_k(t) - \lambda_h > \phi'_{k-1}(t) + \lambda_h, t \in \mathbb{R}, 2 \leq k \leq K, \quad (6)$$

then $Z_k \cap Z_\ell = \emptyset, k \neq \ell$, which means the components of $x(t)$ are well separated in the time-frequency plane. (6) is a required condition for the study of FSST in [35] and for the study of the second-order FSST in [37]. This was also pointed in [42], namely if the STFTs of two components are mixed, the corresponding FSSTs will not be able to separate these two components too. This is also true for other linear time-frequency analysis methods, such as continuous wavelet transform (CWT) and CWT-based SSTs (see [5, 42]).

[4] introduced signal separation operator (SSO) for signal IF estimation and component recovery of multicomponent signals. More precisely, let $h(t)$ be an admissible window function which is nonnegative and even on \mathbb{R} , in $C^3(\mathbb{R})$, $\text{supp}(h) \subseteq [-1, 1]$ and $h(t) \neq 0$. For $a > 0$, denote

$$\hbar_a := \sum_{n \in \mathbb{Z}} h\left(\frac{n}{a}\right). \quad (7)$$

When a is large enough, then $\hbar_a > 0$. The SSO $T_{a, \delta}$ in (1) is defined as

$$(T_{a, \delta} x)(t, \theta) := \frac{1}{\hbar_a} \sum_{n \in \mathbb{Z}} x(t - n\delta) h\left(\frac{n}{a}\right) e^{j2\pi n\theta}, \quad (8)$$

where h is an admissible window function, $\delta, a > 0$ are parameters.

[4] established that, under certain conditions on $A_k(t), \phi_k(t)$, when the components of $x(t)$ are well-separated with $(T_{a, \delta} x)(t, \theta)$, then the ridge $\widehat{\theta}_{k, t}$ on the $(T_{a, \delta} x)(t, \theta)$ plane corresponding to the IF of the sub-signal $x_k(t)$ gives an approximation to the IF $\phi'_k(t)$. In addition, the sub-signal $x_k(t)$ can be recovered directly by

$$\widehat{x}_k(t) = 2\Re e(T_{a, \delta} x)(t, \widehat{\theta}_{k, t}).$$

The reader is referred to [4] for the details. In the next section, we introduce adaptive SSO and its relationship to the STFT with a time-varying parameter, termed as the adaptive STFT, considered in [39].

3 Adaptive signal separation operator (ASSO)

In this section, first for the purpose to recover a complicated non-stationary signal as modeled in (1), we introduce the adaptive signal separation operator with time-varying parameter for each signal

component. After that we show the relationship between ASSO and the adaptive STFT considered in [39]. Finally, we consider the well-separated conditions.

3.1 ASSO

Definition 1. (*Adaptive signal separation operator, ASSO*). Let $x(t)$ be a signal given by (1). For each sub-signal x_k in (1), let $a_{k,t} > 0$ be a time-varying parameter depending on $\phi'_k(t)$ and its neighboring IFs $\phi'_{k-1}(t)$ and $\phi'_{k+1}(t)$. The (modified) adaptive signal separation operator (ASSO) $T_{a_{k,t}}^\delta$ applied to x is defined by

$$(T_{a_{k,t}}^\delta x)(t, \eta) := \frac{1}{\tilde{h}_{a_{k,t}}} \sum_{n \in \mathbb{Z}} x(t - n\delta) h\left(\frac{n}{a_{k,t}}\right) e^{j2\pi\delta n\eta}, \quad (9)$$

where h is an admissible window function, $\delta > 0$ and $a_{k,t} > 0$ are parameters, with $a_{k,t}$ large enough such that $\tilde{h}_{a_{k,t}}$ defined by (7) with $a = a_{k,t}$ is positive.

Note that compared with SSO, ASSO uses a time-varying parameter $a_{k,t} > 0$ which depends on $\phi'_k(t)$ and its neighboring IFs $\phi'_{k-1}(t)$ and $\phi'_{k+1}(t)$. In addition, θ in (8) is replaced by $\delta\eta$. Thus the restriction in [4] for θ : $\theta \in [0, \pi]$ is released. Namely, there is no restriction on the frequency variable η .

In the following we also assume $\int_{\mathbb{R}} h(t)dt = 1$. In addition, we assume the signals $x(t)$ given by (1) satisfy the following conditions, termed as Assumption 1.

Assumption 1. For the non-stationary real signal $x = x(t)$ in (1), we assume that $A_0 \in C^0$, $0 < A_k \in C^1$, $\phi_k \in C^2$, $k = 1, \dots, K$ and $\phi'_k > \phi'_{k-1} > 0$, $k = 2, \dots, K$, and that there exists a constant $\varepsilon > 0$ such that for small u ,

$$\begin{aligned} |\phi'_k(t+u) - \phi'_k(t)| &\leq \varepsilon|u| \phi'_k(t), \\ |A_k(t+u) - A_k(t)| &\leq \varepsilon|u| A_k(t), \quad t \in \mathbb{R}. \end{aligned} \quad (10)$$

Denote

$$B = B(t) := \max_{1 \leq k \leq K} \phi'_k(t), \quad \mu = \mu(t) := \min_{1 \leq k \leq K} A_k(t).$$

Then the following theorem for representation and recovery of the k -th sub-signal $x_k(t)$ in (1) can be followed by Theorem 2.4 in [4].

Theorem 1. Let $x(t)$ be a non-stationary signal in (1) satisfying Assumption 1. Let $\delta = \frac{1}{\varepsilon a_{k,t} \sqrt{4B}}$. Then the following statements hold for sufficiently small $\varepsilon > 0$.

(a) The set $\{\eta : |(T_{a_{k,t}}^\delta x)(t, \eta)| > \mu/2\}$ is a disjoint union of some non-empty sets. There exists a set \mathcal{G}_k with $\mathcal{G}_k \subset \{\eta : |(T_{a_{k,t}}^\delta x)(t, \eta)| > \mu/2\}$ and only containing ϕ'_k .

(b) Let

$$\tilde{\eta} = \tilde{\eta}(t) := \arg \max_{\eta \in \mathcal{G}_k} |(T_{a_{k,t}}^\delta x)(t, \eta)|. \quad (11)$$

Then

$$|\tilde{\eta}(t) - \phi'_k(t)| < C \varepsilon^{\frac{1}{3}}. \quad (12)$$

(c) With $\tilde{\eta}$ given by (11), we have

$$|2\Re e(T_{a_{k,t}}x)(t, \tilde{\eta}) - x_k(t)| \leq D \varepsilon^{\frac{1}{3}}, \quad (13)$$

where C and D depend on the signal $x(t)$ and the window function $h(t)$.

3.2 ASSO and adaptive STFT

The authors of [39] introduced the adaptive STFT. In the following we show that ASSO is a discretization version of the adaptive STFT. More precisely, let $g = g(t), t \in \mathbb{R}$ be a window function with $g(0) \neq 0$ and having certain smoothness and decaying order as $t \rightarrow \infty$. Denote

$$g_\sigma(t) := \frac{1}{\sigma} g\left(\frac{t}{\sigma}\right), \quad (14)$$

where $\sigma > 0$ is a parameter. For a signal $x(t)$, the STFT of $x(t)$ with a time-varying parameter (termed as the adaptive STFT) is defined in [39] as

$$\begin{aligned} (T_\sigma x)(t, \eta) &= (T_{\sigma(t)}x)(t, \eta) \\ &:= \int_{\mathbb{R}} x(\tau) g_{\sigma(t)}(\tau - t) e^{-j2\pi\eta(\tau - t)} d\tau \\ &= \int_{\mathbb{R}} x(t + \tau) \frac{1}{\sigma(t)} g\left(\frac{\tau}{\sigma(t)}\right) e^{-j2\pi\eta\tau} d\tau, \end{aligned} \quad (15)$$

where $\sigma = \sigma(t) > 0$ is a function of t .

Let us return back to the definition of ASSO. Observe that when $a_{k,t}$ is large, we have

$$\tilde{h}_{a_{k,t}} = \sum_{n \in \mathbb{Z}} h\left(\frac{n}{a_{k,t}}\right) \approx a_{k,t} \int_{\mathbb{R}} h(t) dt = a_{k,t},$$

where we have used the assumption $\int_{\mathbb{R}} h(t) dt = 1$. Thus,

$$\begin{aligned} (T_{a_{k,t}}^\delta x)(t, \eta) &\approx \frac{1}{a_{k,t}} \sum_{n \in \mathbb{Z}} x\left(t - (\delta a_{k,t}) \frac{n}{a_{k,t}}\right) h\left(\frac{n}{a_{k,t}}\right) e^{(j2\pi\delta\eta a_{k,t}) \frac{n}{a_{k,t}}} \\ &\approx \int_{\mathbb{R}} x(t - \delta a_{k,t} u) h(u) e^{j2\pi\delta\eta a_{k,t} u} du \\ &= \int_{\mathbb{R}} x(t + \tau) \frac{1}{\delta a_{k,t}} h\left(\frac{\tau}{\delta a_{k,t}}\right) e^{-j2\pi\eta\tau} d\tau, \end{aligned}$$

where the last equality follows from the substitution $\tau = -\delta a_{k,t} u$ and the fact that h is even. Therefore ASSO $(T_{a_{k,t}}^\delta x)(t, \eta)$ is a discretization of the adaptive STFT $(T_\sigma x)(t, \eta)$ with $g = h$ and $\sigma = \delta a_{k,t}$.

In the following, when we discuss the IF estimation (12) and component recovery (13), we will deal with $(T_\sigma x)(t, \eta)$ instead of $(T_{a_{k,t}}^\delta x)(t, \eta)$. We will consider the well-separated condition in the next subsection and component recovery in the next section when g is the Gaussian window function.

3.3 Separation condition analysis

Let

$$g(t) = \frac{1}{\sqrt{2\pi}} e^{-\frac{t^2}{2}}. \quad (16)$$

Then $g_\sigma(t)$ defined by (14) is the Gaussian window function with standard variance σ .

To model a frequency-varying signal more accurately, we consider the local approximation of linear chirps or linear frequency modulation (LFM) signals in this paper. We say $s(t)$ is an LFM signal or a linear chirp if $s(t) = A \cos(2\pi(ct + rt^2/2))$. In this paper we always assume $c + rt > 0$. Then for $\eta > 0$, we have

$$(T_\sigma s)(t, \eta) \approx \frac{A}{2\sqrt{1 - j2\pi\sigma^2 r}} e^{j2\pi(ct + rt^2/2)} m(\eta - (c + rt)), \quad (17)$$

where

$$m(\xi) = e^{-\frac{2\pi^2\sigma^2}{1+(2\pi r\sigma^2)^2}(1+j2\pi\sigma^2 r)\xi^2}, \quad (18)$$

and the root of a complex number $\sqrt{1 - j2\pi\sigma^2 r}$ denotes the value located in the same quadrant as $1 - j2\pi\sigma^2 r$.

The derivations of (17) can be followed from [40]. Indeed, [40] shows that the STFT of $\tilde{s}(t) = Ae^{j2\pi(ct + rt^2/2)}$, the complex-version of $s(t)$, is

$$(T_\sigma \tilde{s})(t, \eta) = \frac{\tilde{s}(t)}{\sqrt{1 - j2\pi\sigma^2 r}} m(\eta - (c + rt)).$$

Therefore, the STFT of $\bar{s}(t) = Ae^{-j2\pi(ct + rt^2/2)}$ is

$$(T_\sigma \bar{s})(t, \eta) = \frac{\bar{s}(t)}{\sqrt{1 + j2\pi\sigma^2 r}} m(\eta + (c + rt)).$$

Hence we have

$$(T_\sigma s)(t, \eta) = \frac{1}{2}(T_\sigma \tilde{s})(t, \eta) + \frac{1}{2}(T_\sigma \bar{s})(t, \eta).$$

Observe that $|m(\xi)|$ is a Gaussian function and it approaches to 0 very fast at $\xi \rightarrow \infty$. In addition, $\eta > 0$ and $c + rt > 0$, thus the second term on the right-hand side of the above equation is small and could be negligible, and hence, (17) holds.

Observe that $|m(\xi)|$ gains maximum at $\xi = 0$. Thus the ridge of $(T_\sigma s)(t, \eta)$ concentrates around $\eta = c + rt$ in the time-frequency plane. Hence if $|m(\xi)|$ is *essentially supported* in $[-\lambda_m, \lambda_m]$ for some $\lambda_m > 0$, then $(T_\sigma s)(t, \eta)$ lies in the time-frequency zone given by

$$\{(t, \eta) : |\eta - (c + rt)| < \lambda_m, t \in \mathbb{R}\}.$$

Recall that we say $|m(\xi)|$ is *essentially supported* in $[-\lambda_m, \lambda_m]$ if

$$|m(\xi)| / \max_\xi |m(\xi)| \leq \tau_0, \quad (19)$$

for all $|\xi| \geq \lambda_m$, where τ_0 is a given threshold with $0 < \tau_0 < 1$. For m given by (18), we have

$$\lambda_m = \sqrt{2|\ln \tau_0|} \sqrt{\frac{1}{(2\pi\sigma)^2} + (r\sigma)^2}. \quad (20)$$

When $x_k(t) = A_k(t) \cos(2\pi\phi_k(t))$ with $A_k(t) > 0$, $\phi'_k(t) > 0$ in (2) is well approximated by LFM functions during any local time of $t \in \mathbb{R}$, that is,

$$x_k(t+u) \approx A_k(t) \cos(2\pi(\phi_k(t) + \phi'_k(t)u + \phi''_k(t)u^2/2)), \quad (21)$$

for small u , then analogously, for $\eta > 0$, we have

$$(T_\sigma x_k)(t, \eta) \approx \frac{A_k(t)}{2\sqrt{1 - j2\pi\sigma^2\phi''_k(t)}} e^{j2\pi\phi_k(t)} m_k(\eta - \phi'_k(t)), \quad (22)$$

where in this case,

$$m(\xi) = e^{-\frac{2\pi^2\sigma^2}{1+(2\pi\phi''_k(t)\sigma^2)^2}(1+j2\pi\sigma^2\phi''_k(t))\xi^2}. \quad (23)$$

Thus $(T_\sigma x_k)(t, \eta)$ lies in the time-frequency zone given by

$$\mathcal{Z}_k := \{(t, \eta) : |\eta - \phi'_k(t)| < \lambda_{k,t}, t \in \mathbb{R}\},$$

where

$$\lambda_{k,t} := \sqrt{2|\ln \tau_0|} \sqrt{\frac{1}{(2\pi\sigma)^2} + (\phi''_k(t)\sigma)^2}. \quad (24)$$

If

$$\phi'_k(t) - \phi'_{k-1}(t) > \lambda_{k,t} + \lambda_{k-1,t}, t \in \mathbb{R}, \quad (25)$$

for all $2 \leq k \leq K$, then the components of $x(t)$ are well separated in the time-frequency plane of STFT, namely, $\mathcal{Z}_k, 1 \leq k \leq K$, do not overlap. Based on (25), $x_k(t)$ can be recovered by STFT or the FSSTs-based methods introduced in Section 1.

On the other hand, when using SSO to extract sub-signal $x_k(t)$, we care more about the ridges on the the time-frequency plane. Hence there exists some $w_{k,t}$ satisfying

$$\max\{\lambda_{k,t}, \lambda_{k-1,t}\} \leq w_{k,t} < \lambda_{k,t} + \lambda_{k-1,t}, \quad (26)$$

so that when

$$\phi'_k(t) - \phi'_{k-1}(t) > w_{k,t}, t \in \mathbb{R}, 2 \leq k \leq K, \quad (27)$$

there are K separated ridges on the time-frequency plane corresponding to the IFs $\phi'_k(t), k = 1, 2, \dots, K$, respectively. Then the components of $x(t)$ can be recovered by SSO.

Note that the threshold τ_0 to define the *essential support* $\lambda_{k,t}$ is small enough, which guarantees $w_{k,t}$ satisfying (26) exist. On the one hand, in (26), $w_{k,t} < \lambda_{k,t} + \lambda_{k-1,t}$ means we allow the mixture of $x_{k-1}(t)$ and $x_k(t)$ on the STFT plane. On the other hand, $w_{k,t} \geq \max\{\lambda_{k,t}, \lambda_{k-1,t}\}$ means $w_{k,t}$ should be great enough to make sure the values on the ridge (extrema) of $(T_\sigma x_k)(t, \eta)$ cannot be

disturbed by other components and it should not result in new ridges (artifact components) on the STFT plane.

Here we call (25) and (27) the LFM signal model-based well-separated conditions for $x(t)$. Since for $k = 1, 2, \dots, K$ and $t \in \mathbb{R}$, we have

$$\lambda_{k,t} \geq \lambda_{g_\sigma},$$

where $\text{supp}(\widehat{g}_\sigma) \subseteq [-\lambda_{g_\sigma}, \lambda_{g_\sigma}]$, the equality only holds for stationary signals. The proposed LFM signal model-based well-separated condition is stricter than the sinusoidal signal model-based well-separated condition in (6). Meanwhile, (26) shows SSO is more efficient to separate components with close IFs than STFT and SSTs.

4 Signal separation with ASSO

4.1 Component recovery formula with ASSO

As discussed in Section 3.1, if the non-stationary signal $x(t)$ in (1) satisfies (26), then the components of $x(t)$ can be recovered or reconstructed. Theorem 1 also provides the error bound of ASSO-based component recovery. In this section, we discuss this error bound when g is the Gaussian window function given by (16).

Suppose $x(t) = f(t) + A_0(t)$, where $f(t) = A(t) \cos(2\pi\phi(t))$ is monocomponent. Let

$$\theta^r(t) := \arg \max_{\theta \in \mathcal{G}_f} |(T_\sigma x)(t, \theta)|, \quad (28)$$

where \mathcal{G}_f is defined similarly as \mathcal{G}_k in Theorem 1. We will provide an algorithm to find $\theta^r(t)$ in Section 4. By Theorem 1, we know $f(t)$ can be recovered by

$$f^r(t) = 2\Re\{(T_\sigma x)(t, \theta^r(t))\}. \quad (29)$$

In addition, Theorem 1 provides the frequency estimation error $|\theta^r(t) - \phi'(t)|$ and the function recovery error $|f^r(t) - f(t)|$.

In this paper, we use the following formula to recover the trend $A_0(t)$:

$$A_0^r(t) = \Re\{(T_\sigma x)(t, 0)\}. \quad (30)$$

Note that in the above formulas (28)-(30), we assume $f(t)$ and $A_0(t)$ are well-separated on the STFT plane. Actually, by (15), we have

$$\begin{aligned} A_0^r(t) &= \Re\{(T_\sigma x)(t, 0)\} \approx (T_\sigma A_0)(t, 0) \\ &= \int_{\mathbb{R}} A_0(\tau) g_\sigma(\tau - t) d\tau. \end{aligned} \quad (31)$$

Observe that $A_0^r(t)$ is the filtered result of $A_0(t)$ with filter $g_\sigma(t)$. The recovery error is

$$\begin{aligned}
|A_0^r(t) - A_0(t)| &= \left| \int_{\mathbb{R}} A_0(\tau) g_\sigma(\tau - t) d\tau - A_0(t) \right| \\
&= \left| \int_{\mathbb{R}} A_0(t + \tau) g_\sigma(\tau) d\tau - A_0(t) \right| \\
&= \left| \int_{\mathbb{R}} (A_0(t + \tau) - A_0(t)) g_\sigma(\tau) d\tau \right| \\
&\leq \int_{\mathbb{R}} |(A_0(t + \tau) - A_0(t))| g_\sigma(\tau) d\tau \\
&\leq \int_{\mathbb{R}} \epsilon |\tau A_0(t)| g_\sigma(\tau) d\tau \\
&= \sqrt{\frac{2}{\pi}} |A_0(t)| \epsilon \sigma.
\end{aligned}$$

Note that we assume $|(A_0(t + \tau) - A_0(t))| \leq \epsilon |\tau A_0(t)|$, which is consistent with (10) when $k = 0$. So that we should choose a small σ to recover the trend to obtain a small recovery error.

The objective of this paper is to deal with signals with fast-varying IFs. We assume the components of a multicomponent non-stationary signal can be well approximated by LFMs. More precisely, suppose $f(t)$ can be well-approximated by LFMs as in (21). When g is the Gaussian window function given by (16), by (22), we have $\theta^r(t) \approx \phi'(t)$. Hence, by (22) again,

$$\begin{aligned}
(T_\sigma f)(t, \theta^r(t)) &\approx \frac{A(t)}{2\sqrt{1-j2\pi\sigma^2\phi''(t)}} e^{j2\pi\phi(t)} m(0) \\
&= \frac{A(t)e^{j2\pi\phi(t)}}{2\sqrt{1-j2\pi\sigma^2\phi''(t)}}.
\end{aligned}$$

Thus the component recovery error is

$$\begin{aligned}
e_f &= |f^r(t) - f(t)| \\
&= \left| 2\Re\{(T_\sigma f)(t, \theta^r(t))\} - A(t) \cos(2\pi\phi(t)) \right| \\
&\leq \left| 2(T_\sigma f)(t, \theta^r(t)) - A(t)e^{j2\pi\phi(t)} \right| \\
&\approx \left| \frac{A(t)e^{j2\pi\phi(t)}}{\sqrt{1-j2\pi\sigma^2\phi''(t)}} - A(t)e^{j2\pi\phi(t)} \right| \\
&= A(t) \left| \frac{1}{\sqrt{1-j2\pi\sigma^2\phi''(t)}} - 1 \right| \\
&= A(t) \left| \frac{j2\pi\sigma^2\phi''(t)}{\sqrt{1-j2\pi\sigma^2\phi''(t)}(\sqrt{1-j2\pi\sigma^2\phi''(t)}+1)} \right| \\
&\leq \frac{2\pi\sigma^2|\phi''(t)|A(t)}{(1+4\pi^2\sigma^4\phi''^2(t))^{\frac{1}{4}} (1+\sqrt{1+4\pi^2\sigma^4\phi''^2(t)})^{\frac{1}{2}}},
\end{aligned} \tag{32}$$

where the last inequality follows from

$$|\sqrt{1-j2\pi\sigma^2\phi''(t)}+1| \geq (1+\sqrt{1+4\pi^2\sigma^4\phi''^2(t)})^{\frac{1}{2}}.$$

Thus e_f is essentially bounded by $2\pi\sigma^2|\phi''(t)|A(t)$. Note that $e_f \rightarrow 0$ for harmonic components with $\phi''(t) = 0$.

To decrease the reconstruction error in (32), we consider to construct a modified recovery formula and need to use a time-varying $\sigma = \sigma(t)$ for each component $x_k(t)$. Consider the requirement of separating multicomponent signal with close IFs, we try to find a $\sigma(t)$ with the sharpest representation of each component first.

By (20), the sharpest representation of $f(t)$, namely the minimal λ_m is obtained when

$$\sigma = \sigma(t) = \frac{1}{\sqrt{2\pi|\phi''(t)|}}. \tag{33}$$

With the σ defined by (33), the $f(t)$ should be reconstructed by

$$f^r(t) = 2\Re \left\{ \sqrt{1-j} (T_\sigma f)(t, \theta^r) \right\}. \quad (34)$$

Compared to (29), (34) is a modified recovery formula with $\sigma(t) = \frac{1}{\sqrt{2\pi|\phi''(t)|}}$ ($\phi''(t) \neq 0$). Obviously, the recovery error by (34) is less than that by (29) for LFM modes, especially for large chirp rates $|\phi''(t)|$.

Next we consider a two-component AM-FM signal $s(t)$,

$$\begin{aligned} s(t) &= s_1(t) + s_2(t) \\ &= A_1(t) \cos(2\pi\phi_1(t)) + A_2(t) \cos(2\pi\phi_2(t)), \end{aligned}$$

which can be approximated by two LFM modes for any fixed t as that in (21), where $\phi_1''(t), \phi_2''(t) \neq 0$. If we choose $\sigma(t) = 1/\sqrt{2\pi|\phi_1''(t)|}$, then we have the sharpest ridge of $T_\sigma s_1$.

For accurate recovery of the signal components, we should choose a $\sigma(t)$ as small as possible, since the hypothesis of well-approximation of LFM mode is true only during a narrow enough neighborhood of t for a broadband signal with fast-varying frequency. But on the other hand, when $\phi_1''(t)$ is close to 0, the parameter $\sigma(t)$ will be extremely large. So there is a contradiction between sharp representation and accurate recovery of all signal components.

Hence, as $a_{k,t}$ introduced in Definition 1, we should use a time-varying parameter $\sigma_{k,t} = \sigma_k(t)$ for each signal component $x_k(t)$ in (1) and reconstruct the signal components one by one.

From the derivation of the component recovery error bound (32), observe that for $f(t) = A(t) \cos(2\pi\phi(t))$, we will have smaller error if we use the recovery formula:

$$f^r(t) = 2\Re \left\{ \sqrt{1-j2\pi\sigma^2\phi''(t)} (T_\sigma f)(t, \theta^r(t)) \right\}, \quad (35)$$

where $\theta^r(t)$ is the estimated ridge of $(T_\sigma f)(t, \theta)$.

After we discussed the recovery errors for monocomponent signal, we consider the component recovery of $x(t)$ given by (1). We will reconstruct the component of $x(t)$ one by one, say to recover $x_l(t)$ first, then $x_m(t)$, $l \neq m \in 1, 2, \dots, K$, and so on. When we target a particular component, say $x_k(t)$, we will choose $\sigma(t)$, denoted by $\sigma_{k,t}$ depending only on IFs and their derivatives of $x_{k-1}, x_k(t), x_{k+1}(t)$. More precisely, we will choose $\sigma_{k,t}$ such that $(T_{\sigma_{k,t}} x_{k-1})(t, \eta)$, $(T_{\sigma_{k,t}} x_k)(t, \eta)$, $(T_{\sigma_{k,t}} x_{k+1})(t, \eta)$ lie in non-overlapping time-frequency zones, which can be guaranteed by

$$\phi_k'(t) - \phi_{k-1}'(t) > \lambda_{k,t} + \lambda_{k-1,t}, \quad \phi_{k+1}'(t) - \phi_k'(t) > \lambda_{k+1,t} + \lambda_{k,t}, \quad (36)$$

where $t \in \mathbb{R}$, $\lambda_{k,t}$ is defined by (24). Note for $k = K$, only one inequality in (36) is required; for $k = 1$, $x_1(t)$ and the trend $A_0(t)$ should be well-separated on the ASSO plane, as we mentioned just before (31), namely,

$$\phi_1'(t) > \lambda_{1,t} + \lambda_{0,t}, \quad \phi_2'(t) - \phi_1'(t) > \lambda_{2,t} + \lambda_{1,t}, \quad t \in \mathbb{R}$$

where $\lambda_{0,t} = \lambda_{g_\sigma}$ and $\sigma = \sigma_{1,t}$. With the analysis above, in particular by (35), we propose the following recovery formula for $x_k(t)$:

$$x_k^r(t) = 2\Re \left\{ \sqrt{1-j2\pi\sigma_{k,t}^2 r_{k,t}^r} (T_{\sigma_{k,t}} x)(t, \theta_{k,t}^r) \right\}, \quad (37)$$

where $r_{k,t}^r$ is the estimation of chirp rate $\phi_k''(t)$ and

$$\theta_{k,t}^r = \arg \max_{\theta \in \mathcal{G}_k} |(T_{a_{k,t}} x)(t, \theta)|, \quad (38)$$

with \mathcal{G}_k introduced in Theorem 1. By (32), the component recover error with (37) is

$$\begin{aligned} & |x_k^r(t) - x_k(t)| \\ &= |2\Re\{(T_{\sigma} x_k)(t, \theta_{k,t}^r)\} - A_k(t) \cos(2\pi\phi_k(t))| \\ &\approx |\Re\{A_k(t)e^{j2\pi\phi_k(t)}m(0)\} - A_k(t) \cos(2\pi\phi_k(t))| \\ &= 0. \end{aligned} \quad (39)$$

This shows the efficiency of the new reconstruction formula in (37).

From the above discussion, we should choose the parameter $\sigma_{k,t}$ as the minimum σ for each time t , with which x_k is well-separated from other components on the ASSO plane, namely both of the two inequalities in (36) hold.

Based on the discussions above, we present a signal recovery scheme in Fig.1. First, we extract the trend of the input signal $x(t)$ with a small constant σ , with which the trend is well-represented along $\theta = 0$. Then the trend is extracted by (30). After that, we use the recovering process given by Algorithm 1 to extract the multi AM-FM modes in (2) one by one.

Algorithm 1 Adaptive recovering process

1. **Input:** $s^{(1)}(t)$, initialize $p \leftarrow 1$.
 2. Estimate $\sigma_\rho(t)$ for $s^{(p)}(t)$ with (43).
 3. **While** $\max_{\theta} \{|(T_{\sigma_\rho} s^{(p)})(t, \theta)|\} > \gamma$, **do**
 4. $\theta_\ell(t) \leftarrow \arg \max_{\theta \in \mathcal{G}_p} \{|(T_{\sigma_\rho} s^{(p)})(t, \theta)| > \mu\}$.
 5. Let $\sigma_{p,t} \leftarrow \sigma_\ell(t)$ with Algorithm 2.
 6. $\theta_{p,t}^r = \arg \max_{\theta \in \mathcal{G}_p} |(T_{\sigma_{p,t}} s^{(p)})(t, \theta)|$.
 7. Estimate $r_{p,t}^r$ with (41).
 8. $f_p(t) = 2\Re \left\{ \sqrt{1 - j2\pi\sigma_{p,t}^2 r_{p,t}^r} (T_{\sigma_{p,t}} x)(t, \theta_{p,t}^r) \right\}$.
 9. $s^{(p+1)}(t) = s^{(p)}(t) - f_p(t)$.
 10. $p \leftarrow p + 1$.
 11. Estimate $\sigma_\rho(t)$ for $s^{(p)}(t)$ with (43).
 12. **End While.**
 13. $d(t) = s^{(p)}(t)$.
 14. **Outputs:** sub-signals $\{f_p(t), p = 1, 2, 3, \dots\}$ and the residual $d(t)$.
-

Finally, we obtain the trend, all the possible sub-signals $\{f_p(t), p = 1, 2, 3, \dots\}$ and the residual $d(t)$ of $x(t)$,

$$x(t) = A_0(t) + \sum_p f_p(t) + d(t). \quad (40)$$

Note that with Algorithm 1, the energy of sub-signal $f_p(t)$ are supposed to be greater than that of $f_{p+1}(t), p = 1, 2, 3, \dots$. This is due to the component with maximum power is extracted first in the

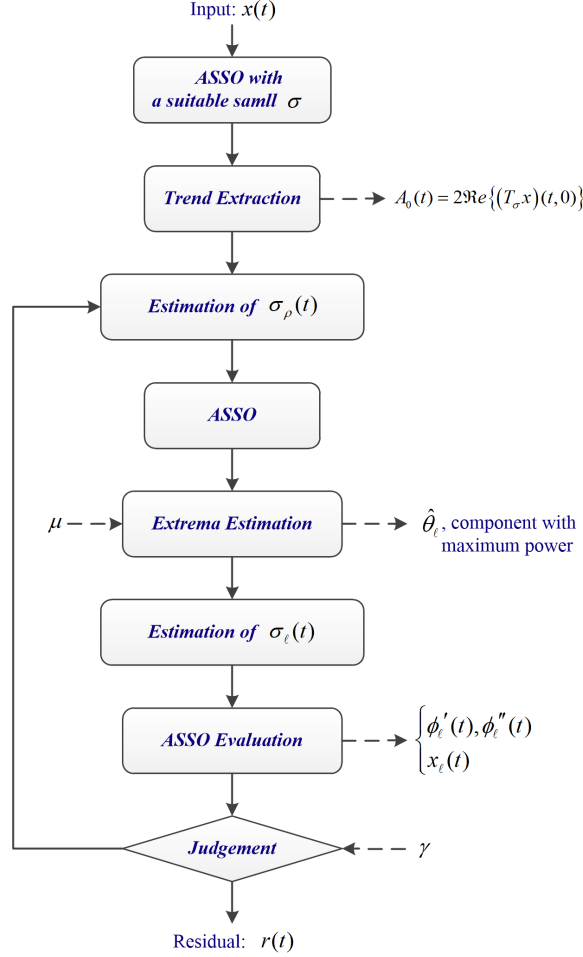


Figure 1: Flowchart diagram for our algorithm.

iterative procedure. The chirp rate estimation $r_{p,t}^r$ is obtained by linear fitting of $\theta_p^r(t)$,

$$\min \|\theta_p^r(u) - (\theta_p^r(t) + r_{p,t}^r u)\|, \quad (41)$$

where $u \in \text{supp}(g_{\sigma_\ell})$. γ and μ are two thresholds for the sake of noises. Usually we let $\gamma > \mu$.

Consider noises and interferences, here we smooth $\sigma_\rho(t)$, $r_{p,t}^r$ and $\sigma_\ell(t)$ in Algorithm 1 with some low-pass filters.

In Algorithm 1, we call $\sigma_\rho(t)$ the global time-varying parameter, with which all components are expect to be well-separated in the ASSO plane. We call $\sigma_\ell(t)$ the local optimal time-varying parameter, with which the component corresponding to $\theta_\ell(t)$ are expect to be well-separated from other components. We will provide the methods to estimate $\sigma_\rho(t)$ and $\theta_\ell(t)$ in the following subsection.

4.2 Estimation of the time-varying parameter

Suppose $x(t)$ given by (1) is separable, meaning (27) holds for all $k = 2, 3, \dots, K$. If we know $\phi_k'(t)$ and $\phi_k''(t)$ for $k = 1, 2, \dots, K$, then we can choose a minimum $\sigma_k(t)$ satisfying (36) to obtain an accurate

recovery of $x_k(t)$. However in practice, we in general have no prior knowledge of $\phi'_k(t)$ and $\phi''_k(t)$. Hence, we need to have methods which provide suitable estimations of $\sigma_\rho(t)$ and $\sigma_\ell(t)$ in Algorithm 1. First, we propose an algorithm to estimate the time-varying parameter $\sigma_\rho(t)$ based on the Rényi entropy.

The Rényi entropy is a commonly used measurement to evaluate the concentration of a time-frequency representation such as STFT in (3), Wigner-Ville distribution[20] (WVD), SST etc. of a signal of $x(t)$, see [43, 44, 46, 45, 40].

In this paper, we define the local Rényi entropy for $\mathcal{T}(t, \theta) = (T_{\sigma, \delta}x)(t, \theta)$ as

$$E_{\zeta, \sigma}(t) := 5 \log_2 \int_{t-\zeta}^{t+\zeta} \int_0^\infty |\mathcal{T}(b, \theta)|^2 d\theta db - 2 \log_2 \int_{t-\zeta}^{t+\zeta} \int_0^\infty |\mathcal{T}(b, \theta)|^5 d\theta db, \quad (42)$$

where ζ is the localization parameter to determine the length of local time. One may refer to [43] for other measures of time-frequency concentrations. Note that the smaller the Rényi entropy, the better the time-frequency resolution. So for a fixed time t and parameter ζ , we can use (42) to find a σ_ρ (denoted as $\sigma_\rho(t)$), which is called the global time-varying parameter in Algorithm 1, with the best time-frequency concentration of $(T_{\sigma_\rho}x)(t, \theta)$. Then, we obtain

$$\sigma_\rho(t) = \operatorname{argmin}_{\sigma > 0} \{E_{\zeta, \sigma}(t)\}. \quad (43)$$

Next, we use Algorithm 2 to search for the local optimal time-varying parameter $\sigma_\ell(t)$. Remember that we should choose a $\sigma(t)$ as small as possible for an accurate recovery of the signal component. Let $\Delta_\sigma > 0$ denote the increment of σ , $\sigma_{min} > 0$ is the minimum value of σ , $s(t)$ is the signal to be processed.

In Algorithm 2, for $\theta_{t,0}$, we find its nearest left local maximum (left peak) with $\theta_{t,-1}$ and nearest right local maximum (right peak) with $\theta_{t,1}$ on $z_t(\theta)$, satisfying $z_t(\theta_{t,-1}) > \mu$ and $z_t(\theta_{t,1}) > \mu$. If there are no such local extrema, viz. no $\theta_{t,-1}$ or $\theta_{t,1}$ above, let $\theta_{t,-1} = 0$ or $\theta_{t,1} = F_s/2$, where F_s is sampling rate of the discrete signal. $[\lambda_l^{(q)}, \lambda_r^{(q)}]$ denotes the support zone of $z_t(\theta)$ around $\theta_{t,0}$, which can be obtained directly by the definition of support zone in this paper, see (19) for example. \mathcal{G}_p in Algorithm 1 and 2 is defined as that in Theorem 1.

5 Numerical experiments

In this section, we provide some numerical examples to further illustrate the effectiveness and robustness of our method in the IF estimation and sub-signal reconstruction.

5.1 LFM modes

First we consider a two-component LFM signal with a trend,

$$\begin{aligned} s(t) &= s_1(t) + s_2(t) + A_0(t) \\ &= \frac{1}{2} \cos(2\pi(17t + 37t^2/2)) + 2 \cos(2\pi(31t + 171t^2/2)) \\ &\quad + (2 + 2 \cos(2\pi t(t - 1/4) - \pi)), \end{aligned} \quad (44)$$

Algorithm 2 Searching for the local optimal parameter

1. **Input:** $s(t)$, initialize $q \leftarrow 1$.
 2. Estimate $\sigma_\rho(t)$ for $s(t)$ with (43).
 3. $\sigma_\ell(t) \leftarrow \sigma_\rho(t)$.
 4. $z_t(\theta) \leftarrow |(T_{\sigma_\ell} s)(t, \theta)|$.
 5. $\theta_{t,0} \leftarrow \arg \max_{\theta \in \mathcal{G}_p} \{|z_t(\theta)| > \mu\}$.
 6. Find $\theta_{t,-1}, \theta_{t,1}, \lambda_l^{(q)}$ and $\lambda_r^{(q)}$ around $\theta_{t,0}$ on $z_t(\theta)$.
 7. **While** $\lambda_l^{(q)} > \theta_{t,-1}$ & $\lambda_r^{(q)} < \theta_{t,1}$ & $\sigma_\ell(t) > \sigma_{min}$, **do**
 8. $\sigma_\ell(t) \leftarrow \sigma_\ell(t) - \Delta_\sigma$.
 9. $q \leftarrow q + 1$.
 10. $z_t(\theta) \leftarrow |(T_{\sigma_\ell} s)(t, \theta)|$.
 11. $\theta_{t,0} \leftarrow \arg \max_{\theta \in \mathcal{G}_p} \{|z_t(\theta)| > \mu\}$.
 12. Find $\lambda_l^{(q)}$ and $\lambda_r^{(q)}$ around $\theta_{t,0}$ on $z_t(\theta)$.
 13. **End While.**
 14. **Output:** $\sigma_\ell(t)$.
-

where $t \in [0, 1]$ for $s_1(t)$ and $s_2(t)$, $t \in [1/4, 3/4]$ for $A_0(t)$. The number of sampling points is $N = 512$ and the sampling rate is 512Hz. The IFs of $s_1(t)$ and $s_2(t)$ are $\phi_1'(t) = 17 + 37t$ and $\phi_2'(t) = 31 + 171t$, respectively. Hence, the chirp rates of $s_1(t)$ and $s_2(t)$ are $\phi_1''(t) = 37$ and $\phi_2''(t) = 171$, respectively. For comparison, in this and the following experiments, we also show some results of the CWT-based SST (WSST) in [5], the second-order CWT-based SST (WSST2) in [31], the STFT-based SST (FSST) in [35], the second-order STFT-based SST (FSST2) in [37] and the EMD and its corresponding Hilbert-Huang Transform in [7].

Fig. 2 shows the original waveform and some recovery results of the trend $A_0(t)$ when $\sigma = 0.02$. Observe that the trends recovered by FSST and FSST2 are not as smooth and accurate as the proposed method in this paper. This is because of the nonlinear operations in FSST and FSST2. Since WSST and WSST2 can not be used for trend extraction, we just consider signals after trend removal in the following experiments.

We will use Algorithm 1 and Algorithm 2 to estimate the adaptive parameters and extract the sub-signals one by one. First we estimate the global time-varying parameter $\sigma_\rho(t)$, with which all components are expect to be well-separated in the ASSO plane. Since $s_2(t)$ is larger than $s_1(t)$ in power, so $s_2(t)$ will be extract firstly with an estimated local optimal time-varying parameter $\sigma_\ell(t)$. After that, $s_1(t)$ will be extracted similarly. Fig.3 shows the IF estimation results of the ASSO method proposed in this paper and other methods. For WSST, WSST2, FSST and FSST2, the IF estimations are base on curve fitting of the ridges on the corresponding time-frequency planes. For EMD, the IFs are estimated by the Hilbert transform of the IMFs and then with a low-pass filter. All methods can recover the two IFs of signal $s(t)$ but with different precision. Observed that the results of ASSO, WSST2 and FSST2 are more precise than those of WSST, FSST and EMD.

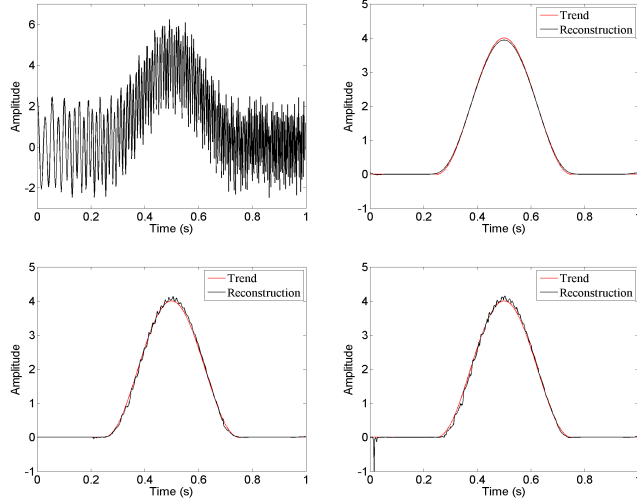


Figure 2: Example of the two-component LFM signal. Top-left: Waveform of $s(t)$; Top-right: Trend recovered by our method when $\sigma = 0.02$; Bottom-left: Trend recovered by FSST when $\sigma = 0.02$; Bottom-right: Trend recovered by FSST2 when $\sigma = 0.02$.

Fig.4 demonstrates the reconstruction results of sub-signal $s_1(t)$ and $s_2(t)$ with the ASSO, WSST2 and FSST2, respectively. We also plot the true waveforms $s_1(t)$ or $s_2(t)$ on each picture. If the reconstructed and the true waveforms are overlapped, then the reconstructed result is good. Observe that our method is better than others for both $s_1(t)$ (Component 1) and $s_2(t)$ (Component 2).

To evaluate the reconstruction errors, we adopt the relative root of mean square error (RMSE), defined as,

$$\text{RMSE}_v = \frac{\|v - \hat{v}\|_2}{\|v\|_2}, \quad (45)$$

where v is a vector and \hat{v} is an estimation of v . Hence, $v = \phi'_k(t)$ for Fig.3, $v = s_1(t)$ or $v = s_2(t)$ for Fig.4. Fig.5 shows the RMSEs of the methods above. Note that there are phase shifts with WSST and WSST2, especially for $s_2(t)$. In general, our method is superior to other methods both on IF estimation and sub-signal reconstruction.

5.2 Nonlinear FM signal

Next we consider a three-component nonlinear FM signal,

$$\begin{aligned} x(t) &= x_1(t) + x_2(t) + x_3(t) \\ &= \cos(2.7\pi t + 0.4 \cos(3\pi t)) + \frac{2}{3} \cos(4.7\pi t + 0.3 \cos(3\pi t)) \\ &\quad + \frac{1}{2} \cos(6.4\pi t + 0.2 \cos(3\pi t)), \end{aligned} \quad (46)$$

where $t \in [0, 20]$. The number of sampling points is $N = 512$, namely sampling rate is $F_s = 25.6$ Hz. The IFs of $x_1(t)$, $x_2(t)$ and $x_3(t)$ are $\phi'_1(t) = 1.35 - 0.6 \sin(3\pi t)$, $\phi'_2(t) = 2.35 - 0.45 \sin(3\pi t)$ and $\phi'_3(t) = 3.2t - 0.3 \sin(3\pi t)$, respectively.

Fig.6 shows the reconstruction results of $x_1(t)$, $x_2(t)$ and $x_3(t)$ with ASSO and FSST2, respectively. Obviously, the reconstructed waveforms by the proposed ASSO is better than those by FSST2.

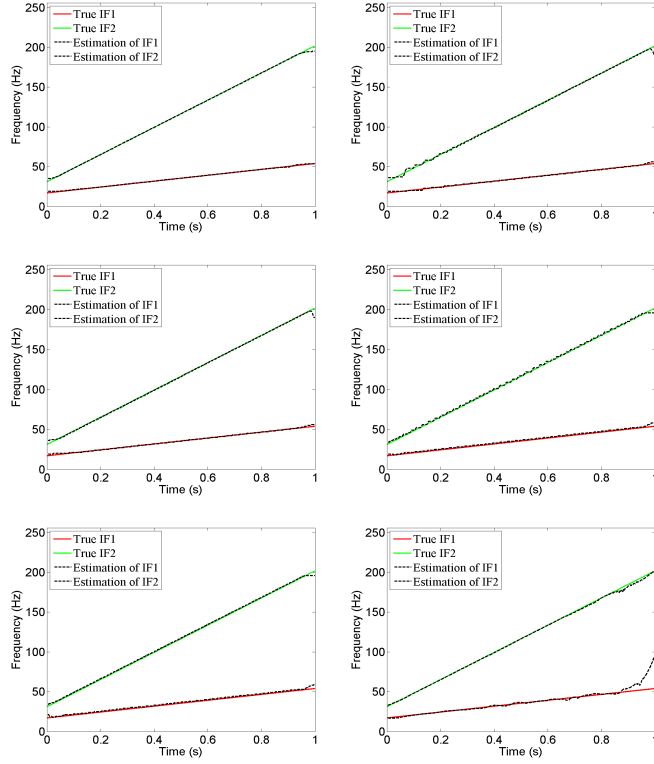


Figure 3: IF estimations of the two-component LFM signal with different methods. Top-left: ASSO; Top-right: WSST; Middle-left: WSST2; Middle-right: FSST; Bottom-left: FSST2; Bottom-right: EMD.

We also use the RMSE to evaluate the errors of IF estimation and waveform reconstruction of all the six methods mentioned in Fig.5, which are shown in Fig.7. Both the results in Fig.5 and Fig.7 demonstrate the correctness and efficiency of our proposed adaptive SSO. Note that for all the experiments in this paper, we use Morlet’s wavelet for WSST and WSST2, and Gaussian window for FSST and FSST2. One may consider use some suitable parameters to improve the results of SSTs. This may work for some non-stationary signals, but still can not separate the fast-varying broadband signals. Because for complicated broadband multicomponent signals, there is no one constant parameter which is fit for all the components.

5.3 Radar echoes

Here we consider the measured data from a conventional low-resolution very-high-frequency (VHF) surveillance radar. The pulse-repetition frequency (PRF) of the radar is 400 Hz. The left picture of Fig.8 shows the data to be processed, which consists of 300 discrete samples. Note that these samples are corresponding to each radar echoes, which means the samples are obtained after the radar signal processing of matched filtering and detection. Therefore the sampling rate in left picture of Fig.8 is equal to the PRF, namely 400Hz.

The middle and right pictures of Fig.8 shows the IF estimation results by ASSO and FSST2, respectively. Observe that there are two frequency components in time-frequency plane. Actually,

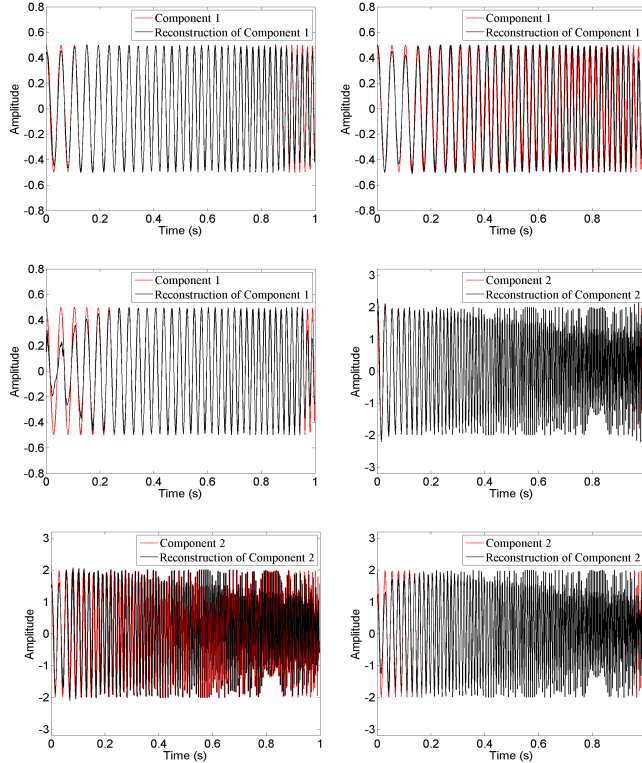


Figure 4: Reconstructions of $s_1(t)$ and $s_2(t)$ with different methods. Top-left: ASSO for $s_1(t)$; Top-middle: WSST2 for $s_1(t)$; Top-right: FSST2 for $s_1(t)$; Bottom-left: ASSO for $s_2(t)$; Bottom-middle: WSST2 for $s_2(t)$; Bottom-right: FSST2 for $s_2(t)$.

the data here is collected when two targets in formation fly past the radar. The IFs are corresponding to the Doppler frequencies aroused the changes of targets' aspects and speeds with respect to the radar. Since the two targets in formation are close, they are located at the same range unit of the conventional low-resolution radar. It is hardly to distinguish the two targets and estimate their Doppler frequencies by conventional Fourier-based methods. It shows the Doppler frequency of aerial target varies approximate linearly and smoothly in [47]. To be fair, the window parameters σ for FSST2 is equal to the average value of the global time-varying parameter $\sigma_\rho(t)$ estimated in Step a of Algorithm 1. All the IFs in Fig.8 are estimated by the ridges directly (without curving fitting). Observe that the results of our method are much smoother than those of FSST2.

5.4 Bat signal

Finally, we test our method on a bat echolocation signal emitted by a large brown bat (*Eptesicus Fuscus*) in real world. Fig.9 shows the waveform and spectrum of the Bat echolocation signal. There are 400 samples with the sampling period 7 microseconds (sampling rate $F_s \approx 142.86$ KHz). The data can be downloaded from the website of DSP at Rich University: <http://dsp.rice.edu/software/bat-echolocation-chirp>[48].The IF representation of this bat signal has studied in [30], [32] by second-order FSST and the instantaneous frequency-embedded synchrosqueezing wavelet transform (IF-

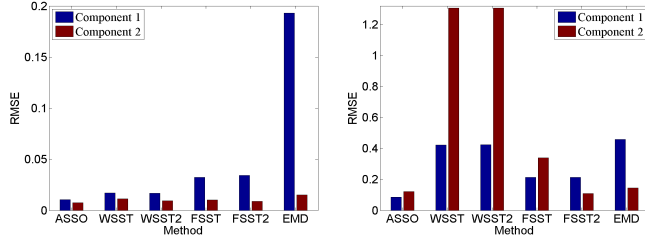


Figure 5: Performance comparisons of different methods. Left: The RMSE of IF estimation; right: The RMSE of sub-signal reconstruction.

SST) respectively. From the results in [30] and [32], we know the bat echolocation signal is consist of four components, and all the components are approximated to LFM modes.

Fig.10 shows the results of IF estimation and waveform reconstruction. Observe that the four components are decomposed clearly. Different from the ridge detection method in [30], which assumes the number of components is known, we extract each ridge by the local maxima without any prior knowledge. And by Algorithm 1, our method is adaptive and automatically. We can process sub-signals which are time staggered.

6 Conclusion

In this paper, we introduce a direct signal separation method via extraction of local frequencies. The proposed method works like the EMD approach, can separate complicated multicomponent non-stationary signal adaptively and automatically without any prior knowledge. By the approximation of LFM modes and derivation of separation conditions, we show the proposed method is capable to separate components with closer IFs than the existing state-of-the-art methods. Moreover, for measured signals, the proposed method can be implemented by FFT, which is suitable for engineering applications. The further study is to consider how to take advantage of the ASSO for separating multicomponent signals with crossings of instantaneous frequency curves.

Acknowledgment

The authors would like to thank Dr. Ningning Han and Prof. Hongbing Ji for helpful discussions.

References

- [1] P. Flandrin and P. Borgnat, “Time-frequency energy distributions meet compressed sensing,” *IEEE Transactions on Signal Processing*, vol. 58, no. 6, pp.2974-2982, Jun 2010.
- [2] F. Gianfelici, G. Biagetti, P. Crippa and C. Turchetti, “Multicomponent AM-FM representations: An asymptotically exact approach,” *IEEE Transactions on Audio, Speech and Language Processing*, vol. 15, no. 3, pp. 823–837, March 2007.

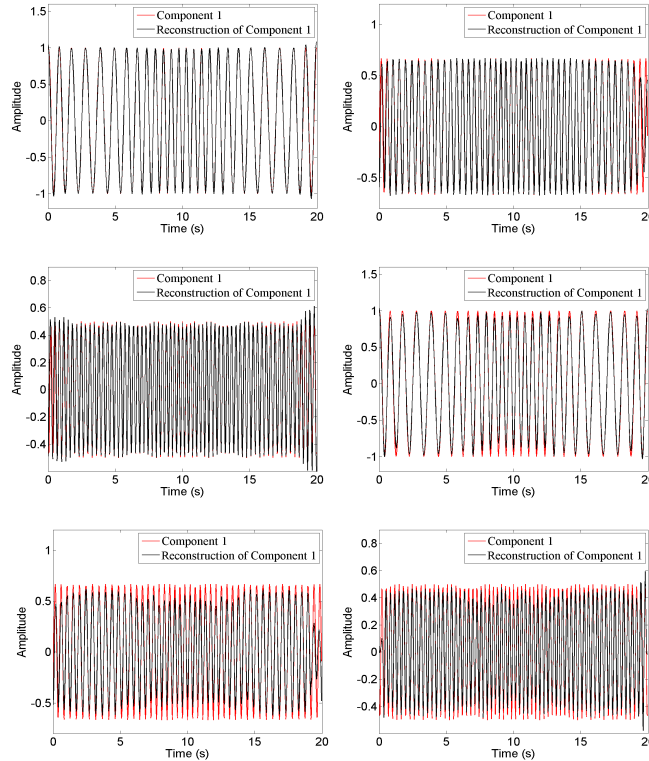


Figure 6: Reconstructions of $x_1(t)$, $x_2(t)$ and $x_3(t)$ with different ASSO and FSST2. Top-left: ASSO for $x_1(t)$; Top-middle: ASSO for $x_2(t)$; Top-right: ASSO for $x_3(t)$; Bottom-left: FSST2 for $x_1(t)$; Bottom-middle: FSST2 for $x_2(t)$; Bottom-right: FSST2 for $x_3(t)$.

- [3] N.E. Huang, Z. Shen, S.R. Long, M.L. Wu, H.H. Shih, Q. Zheng, N.C. Yen, C.C. Tung, and H.H. Liu, “The empirical mode decomposition and Hilbert spectrum for nonlinear and nonstationary time series analysis,” *Proc. Roy. Soc. London A*, vol. 454, no. 1971, pp. 903–995, Mar. 1998.
- [4] C. K. Chui and H. N. Mhaskar, “Signal decomposition and analysis via extraction of frequencies,” *Appl. Comput. Harmon. Anal.*, vol. 40, no. 1, pp. 97–136, 2016.
- [5] I. Daubechies, J. Lu, and H.-T. Wu, “Synchrosqueezed wavelet transforms: An empirical mode decomposition-like tool,” *Appl. Computat. Harmon. Anal.*, vol. 30, no. 2, pp. 243–261, Mar. 2011.
- [6] H.-T. Wu, *Adaptive analysis of complex data sets*, Ph.D. dissertation, Princeton Univ., Princeton, NJ, 2012.
- [7] N. E. Huang and Z. Wu, “A review on Hilbert-Huang transform: Method and its applications to geophysical studies,” *Rev. Geophys.*, vol. 46, no. 2, June 2008.
- [8] P. Flandrin, G. Rilling, and P. Goncalves, “Empirical mode decomposition as a filter bank,” *IEEE Signal Proc. Letters*, vol. 11, pp. 112–114, Feb. 2004.

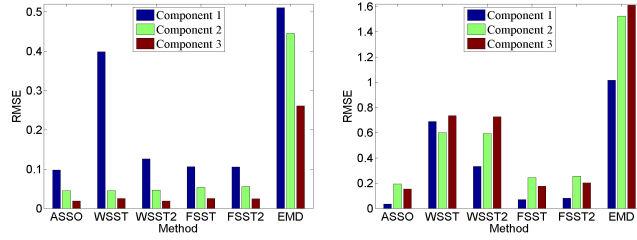
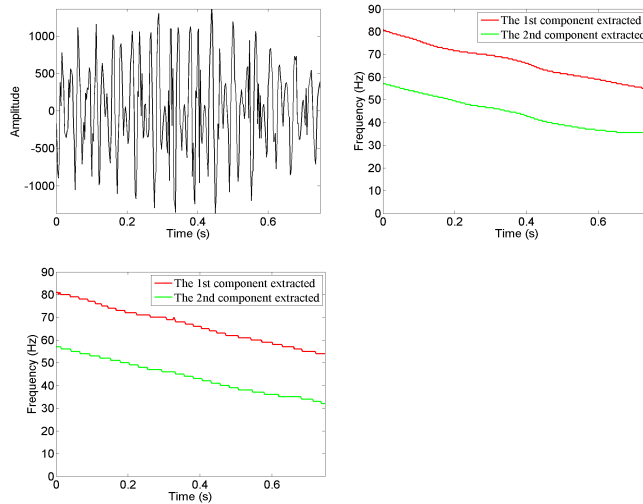


Figure 7: Performance comparisons of different methods for the three-component nonlinear FM signal. Left: The RMSE of IF estimation; right: The RMSE of sub-signal reconstruction.



S

Figure 8: Radar data and its estimation results. Left: The samples of the radar data; Middle: IF estimated by ASSO; Right: IF estimated by FSST2.

- [9] Y. Xu, B. Liu, J. Liu, and S. Riemenschneider, "Two-dimensional empirical mode decomposition by finite elements," *Proc. Roy. Soc. London A*, vol. 462, no. 2074, pp. 3081–3096, Oct. 2006.
- [10] G. Rilling and P. Flandrin, "One or two frequencies? The empirical mode decomposition answers," *IEEE Trans. Signal Proc.*, vol. 56, pp. 85–95, Jan. 2008.
- [11] Z. Wu and N.E. Huang, "Ensemble empirical mode decomposition: A noise-assisted data analysis method," *Adv. Adapt. Data Anal.*, vol. 1, no. 1, pp. 1–41, Jan. 2009.
- [12] L. Li and H. Ji, "Signal feature extraction based on improved EMD method," *Measurement*, vol. 42, pp. 796–803, June 2009.
- [13] T. Oberlin, S. Meignen and V. Perrier, "An alternative formulation for the empirical mode decomposition," *IEEE Trans. Signal Proc.*, vol. 60, no. 5, pp. 2236–2246, May 2012.
- [14] Y. Wang, G.-W. Wei and S.Y. Yang, "Iterative filtering decomposition based on local spectral evolution kernel," *J. Scientific Computing*, vol. 50, no. 3, pp. 629–664, Mar. 2012.

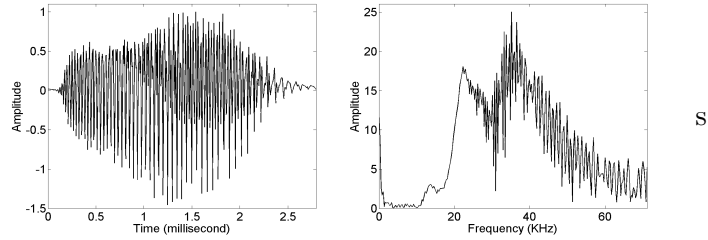


Figure 9: Waveform and spectrum of the bat signal. Left: Waveform; right: Spectrum.

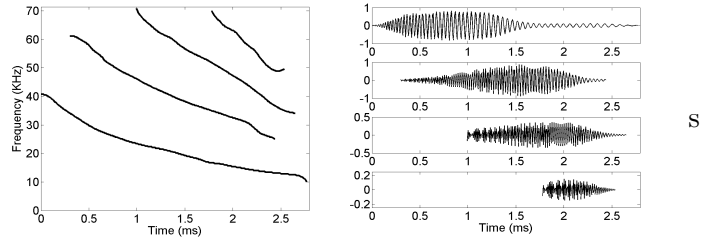


Figure 10: IF estimation and waveform reconstruction of the bat signal. Left: IF estimation; right: Waveform reconstruction.

- [15] A. Cicone, J.F. Liu, and H.M. Zhou, “Adaptive local iterative filtering for signal decomposition and instantaneous frequency analysis,” *Appl. Comput. Harmon. Anal.*, vol. 41, no. 2, pp. 384–411, Sep. 2016.
- [16] L. Li and H. Cai, Q. Jiang and H. Ji, “An empirical signal separation algorithm for multicomponent signals based on linear time-frequency analysis,” *Mechanical Systems and Signal Processing*, vol. 121, no. 4, pp. 791–809, April 2019.
- [17] B. G. R. De Prony, “Essai experimental et analytique: sur les lois de la dilatabilite de fluides elastique et sur celles de la force expansive de la vapeur de lalkool, a differentes temperatures,” *Journal de lecole polytechnique*, vol.1, no. 22, pp. 24 – 76, 1795.
- [18] R.O. Schmidt, “Multiple Emitter Location and Signal Parameter Estimation,” *IEEE Trans. Antennas and Propagation*, vol. 34, no. 3, pp.276–280, Mar. 1986.
- [19] R. Roy and T. Kailath, ”ESPRIT-estimation of signal parameters via rotational invariance techniques,” *IEEE Trans. Acoustics, Speech, and Signal Proc.*, vol. 37, no. 7, pp. 984–995, Jul. 1989.
- [20] L. Cohen, *Time-frequency Analysis*, Prentice Hall, New Jersey, 1995.
- [21] L. Stanković, M. Daković, and T. Thayaparan, *Time-Frequency Signal Analysis with Applications*, Artech House, Boston, 2013.

- [22] I. Daubechies and S. Maes, “A nonlinear squeezing of the continuous wavelet transform based on auditory nerve models,” in A. Aldroubi, M. Unser Eds. *Wavelets in Medicine and Biology*, CRC Press, 1996, pp. 527–546.
- [23] S. Meignen, T. Oberlin, and S. McLaughlin, “A new algorithm for multicomponent signals analysis based on synchrosqueezing: With an application to signal sampling and denoising,” *IEEE Trans. Signal Proc.*, vol. 60, no. 11, pp. 5787–5798, Nov. 2012.
- [24] F. Auger, P. Flandrin, Y. Lin, S. McLaughlin, S. Meignen, T. Oberlin, and H.-T. Wu, “Time-frequency reassignment and synchrosqueezing: An overview,” *IEEE Signal Process. Mag.*, vol. 30, no. 6, pp. 32–41, 2013.
- [25] C. Li and M. Liang, “A generalized synchrosqueezing transform for enhancing signal time-frequency representation,” *Signal Proc.*, vol. 92, no. 9, pp. 2264–2274, 2012.
- [26] G. Thakur, E. Brevdo, N. Fučkar, and H.-T. Wu, “The synchrosqueezing algorithm for time-varying spectral analysis: Robustness properties and new paleoclimate applications,” *Signal Proc.*, vol. 93, no. 5, pp. 1079–1094, 2013.
- [27] C. K. Chui, Y.-T. Lin, and H.-T. Wu, “Real-time dynamics acquisition from irregular samples—with application to anesthesia evaluation,” *Anal. Appl.*, vol. 14, no. 4, pp. 537–590, Jul. 2016.
- [28] C. K. Chui and M. D. van der Walt, “Signal analysis via instantaneous frequency estimation of signal components,” *Int’l J Geomath*, vol. 6, no. 1, pp. 1–42, Apr. 2015.
- [29] H.Z. Yang, “Synchrosqueezed wave packet transforms and diffeomorphism based spectral analysis for 1D general mode decompositions,” *Appl Comput. Harmon. Anal.*, vol. 39, no.1, pp.33–66, 2015.
- [30] S. Meignen, D.-H. Pham, and S. McLaughlin, “On demodulation, ridge detection and synchrosqueezing for multicomponent signals,” *IEEE Trans. Signal Proc.*, vol. 65, no. 8, pp. 2093–2103, Apr. 2017.
- [31] T. Oberlin and S. Meignen, “The 2nd-order wavelet synchrosqueezing transform,” in *2017 IEEE Int. Conf. Acoust., Speech, Signal Process. (ICASSP)*, Mar. 2017, New Orleans, LA, USA, pp. 3994–3998.
- [32] Q. Jiang and B.W. Suter, “Instantaneous frequency estimation based on synchrosqueezing wavelet transform,” *Signal Proc.*, vol. 138, pp.167–181, 2017.
- [33] H.Z. Yang, “Statistical analysis of synchrosqueezed transforms,” *Appl. Comput. Harmon. Anal.*, vol. 45, no. 3, pp. 526–550, Nov. 2018.
- [34] G. Thakur and H.-T. Wu, “Synchrosqueezing based recovery of instantaneous frequency from nonuniform samples,” *SIAM J. Math. Anal.*, vol. 43, pp. 2078–2095, 2011.

- [35] T. Oberlin, S. Meignen, and V. Perrier, “The Fourier-based synchrosqueezing transform,” in *2014 IEEE Int. Conf. Acoust., Speech, Signal Process. (ICASSP)*, May 2014, Florence, Italy, pp. 315–319.
- [36] S. Wang, X. Chen, G. Cai, B. Chen, X. Li, and Z. He, “Matching demodulation transform and synchrosqueezing in time-frequency analysis,” *IEEE Trans. Signal Proc.*, vol. 62, no. 1, pp. 69–84, 2014.
- [37] T. Oberlin, S. Meignen, and V. Perrier, “Second-order synchrosqueezing transform or invertible reassignment? towards ideal time-frequency representations,” *IEEE Trans. Signal Proc.*, vol. 63, no. 5, p.1335–1344, Mar. 2015.
- [38] S.B. Wang, X.F. Chen, I.W. Selesnick, Y.J. Guo, C.W. Tong and X.W. Zhang, “Matching synchrosqueezing transform: A useful tool for characterizing signals with fast varying instantaneous frequency and application to machine fault diagnosis,” *Mechanical Systems and Signal Proc.*, vol. 100, pp. 242–288, Feb. 2018.
- [39] L. Li, H.Y. Cai, H.X. Han, Q.T. Jiang and H.B. Ji, “Adaptive short-time Fourier transform and synchrosqueezing transform for non-stationary signal separation,” *Signal Proc.*, in press. arXiv:1812.11292
- [40] L. Li, H.Y. Cai, and Q.T. Jiang, “Adaptive synchrosqueezing transform with a time-varying parameter for non-stationary signal separation,” *Appl. Comput. Harmon. Anal.*, in press. arXiv:1812.11364.
- [41] Z.-L. Huang, J. Z. Zhang, T. H. Zhao, and Y. B. Sun, “Synchrosqueezing S-transform and its application in seismic spectral decomposition,” *IEEE Trans. Geosci. Remote Sensing*, vol. 54, no. 2, pp. 817–825, Feb. 2016.
- [42] D. Iatsenko, P.-V. E. McClintock and A. Stefanovska, “Linear and synchrosqueezed time-frequency representations revisited: Overview, standards of use, resolution, reconstruction, concentration, and algorithms,” *Digital Signal Proc.*, vol. 42, pp. 1-26, Jul. 2015.
- [43] L. Stankovic, “A measure of some time-frequency distributions concentration,” *Signal Proc.*, vol. 81, no. 3, pp. 621-631, 2001.
- [44] R. Baraniuk, P. Flandrin, A. Janssen, and O. Michel, “Measuring time-frequency information content using the Rényi entropies,” *IEEE Trans. Inform. Theory*, vol. 47, no. 4, pp. 1391–1409, 2001.
- [45] V. Sharma and A. Parey, “Performance evaluation of decomposition methods to diagnose leakage in a reciprocating compressor under limited speed variation,” *Mechanical Systems and Signal Proc.*, in press, 2018, <https://doi.org/10.1016/j.ymssp.2018.07.029>.

- [46] Y.-L. Sheu, L.-Y. Hsu, P.-T. Chou, and H.-T. Wu, “Entropy-based time-varying window width selection for nonlinear-type time-frequency analysis,” *Int’l J. Data Sci. Anal.*, vol. 3, pp. 231–245, 2017.
- [47] L. Li and H. Ji, “Radar targets detection in formation based on time-varying AR model,” in *2006 CIE International Conference on Radar (ICA)*, October 2006, Shanghai, China.
- [48] <http://dsp.rice.edu/software/bat-echolocation-chirp>.